Special Issue: Vesuvius monitoring and knowledge

The first Long Period earthquake detected in the background seismicity at Mt. Vesuvius

Paola Cusano*, Simona Petrosino, Francesca Bianco, Edoardo Del Pezzo

Istituto Nazionale di Geofisica e Vulcanologia, Sezione di Napoli, Osservatorio Vesuviano, Naples, Italy

Article history
Received September 5, 2012; accepted March 11, 2013.
Subject classification:
Volcano seismology, Volcano monitoring, Volcanic event classification, Long Period earthquake, Signal analysis, Hydrothermal system.

ABSTRACT

The typical earthquakes occurring at Mt. Vesuvius are Volcano-Tectonic. On July 20, 2003, an unusual earthquake with low and narrow frequency content was detected. The seismograms presented an emergent onset and a nearly monochromatic spectrum at all stations of the Osservatorio Vesuviano (Istituto Nazionale di Geofisica e Vulcanologia) seismic network. The event was located at about 4 km b.s.l. close to the crater axis and an equivalent duration magnitude of 0.6 was estimated. The nature of this event was investigated by comparing its features with those of two typical Volcano-Tectonic earthquakes occurred inside the same source volume. We compared the spectral content calculating the spectrograms and the coda patterns using the Hilbert Transform. A Seismic Moment Tensor inversion was performed on the low frequency earthquake. The focal mechanisms for the two Volcano-Tectonic earthquakes were estimated with a classical technique and resulted compatible with the stress field acting on the volcano. Taking into account the clear differences with the typical Volcano-Tectonic events as well as the peculiarities retrieved from our analyses (monochromatic, low frequency spectral content, and sustained coda) and also some geochemical observations, we classify the unusual low frequency seismic event detected at Mt. Vesuvius as Long Period earthquake and propose that its origin could be linked to a pressure drop in the deep hydrothermal system.

1. Introduction

Mt. Vesuvius (southern Italy) is considered one of the most dangerous volcano in the world being surrounded by the metropolitan area of Naples. After the last eruption in 1944 the volcano entered a period of quiescence, characterized by low magnitude seismicity and hydrothermal activity. At this stage one of the main tasks of the volcanologists is to reveal the eventual precursors of the next eruption. To this aim it is fundamental the knowledge of the background state of the volcano by studying, identifying and understanding the mechanisms responsible for the recorded signals.

The monitoring and the classification of seismicity can allow the identification of the processes occurring in a volcanic system to gain information about its state and evolution. Following Chouet [1996] it is possible to classify the earthquakes that occur in volcanic environment, at frequencies higher than 1 Hz into two major categories. One category includes Volcano-Tectonic (VT) or High Frequency (HF) quakes, that involve failures in the brittle rock in which fluids do not influence directly the source. Tensile failures produced by thermal contraction belong to this class. The source mechanisms of VTs are similar to those observed for tectonic earthquakes. The other category comprises events in which fluids are actively involved in the source process. Usually they are related to a pressure transient generating resonance of fluid-filled cavities (cracks, conduits, etc.). The source responds with a prolonged ringing (Long Period (LP) earthquakes, and volcanic tremor) at frequencies in 1-5 Hz band [Lahr et al. 1994, Chouet 1996, Neuberg et al. 2000]. Hybrid events, mixing LP and VT quake features, represent the transition between the two categories. Since LP earthquakes and tremor usually precede volcanic eruptions they are largely studied by the scientific community [Lahr et al. 1994, Jolly et al. 2012].

The typical earthquakes occurring at Mt. Vesuvius are low magnitude VTs. Besides these events, the network also detects artificial events, namely quarry blasts and artificial shots, fired in the bay of Naples. These kinds of events are recognized and separated from VT earthquakes on the basis of visual inspection of waveforms and their spectral content [Bianco at al. 2005]. To improve the quality of monitoring in the vesuvian area a temporary small short-period seismic array was installed on the southern flank of Vesuvius (Figure 1) in June 2003 [Bianco et al. 2005].

On July 20, 2003, an unusual low frequency narrow band event was recorded by the Osservatorio Vesu-

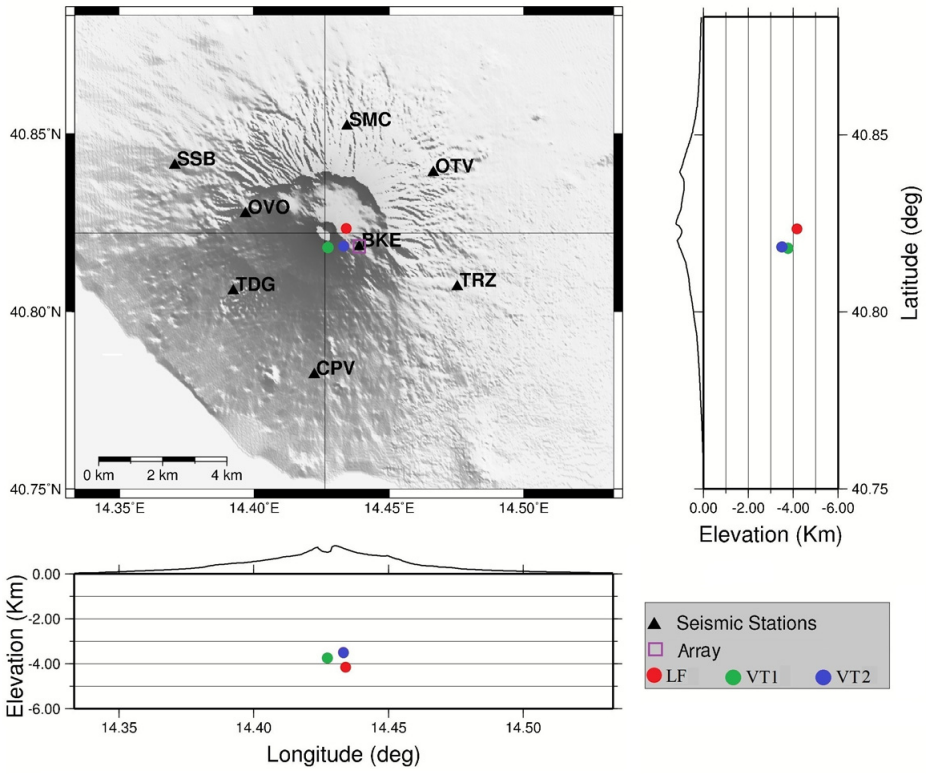

Figure 1. Mt. Vesuvius map, with the position of the seismic stations that recorded at least one of the three analyzed seismic events and the epicenters of these earthquakes according to the legend in the bottom-right corner. On the right side the depth of the three events is represented on the NS-section of the volcanic edifice. The EW-section is shown at the bottom.

viano monitoring network; this event presented a nearly monochromatic spectrum peaked at 3-4 Hz at the stations. Bianco et al. [2005], taking advantage of array techniques to infer the kinematic properties of this event, established its natural and deep origin, and classified it as LP volcanic earthquake, likely linked to magmatic/hydrothermal activity. In the present paper we investigate the dynamical features of this unusual earthquake, on the basis of the results obtained by Bianco et al. [2005], with the aim of contributing to the knowledge of the seismic background state of Mt. Vesuvius in its quiescent stage. After a general overview of the volcanic system, we retrieve the major properties of the LP performing a spectral analysis, a study of the coda pattern, and a Seismic Moment Tensor inversion to infer the source mechanism. At the same time, we perform a quantitative comparison with the typical vesuvian seismicity.

2. Somma-Vesuvius activity

Somma-Vesuvius volcanic complex (southern Italy) is a strato-volcano, 1281 m high above sea level (a.s.l.) and 10 km wide (Figure 1). It hosts the Vesuvius recent cone, grown inside the older Somma caldera. The edifice is interested by two regional normal fault systems, trending NW–SE and NE–SW [Acocella and Funiciello 2006, Di Renzo et al. 2007]. The NW-SE faults involve the north-eastern sector of Somma edifice and the south-western sector of Mt. Vesuvius. The NE-SW structure affects the north-western sector of Mt. Somma, where probably dips to dislocate the Mesozoic carbonatic basement, whose top can be encountered at a mean depth of about 2/2.5 km. Besides these regional structures, the Somma caldera and the southern flank of Mt. Vesuvius are crosscut by local eruptive fractures, trending along EW and NS directions.

In recent epoch, at least 4 plinian eruptions occurred (Pomici di Base, Mercato, Avellino, and Pompei), alternated with moderate activities (sub-plinian eruptions, strombolian activity, lava flows) and quiescent stages [Cioni et al. 1998, De Vivo and Rolandi 2001]. The most recent eruptive stage lasted from 1631 to 1944, and was characterized by a persistent open-conduit activity. The present volcanism consists of low energy seismicity, CO_2 degassing and low-temperature fumarolic activity in the crater area, and thermal submarine features [Chiodini et al. 2001, Caliro et al. 2011].

The current Mt. Vesuvius seismicity consists of low magnitude VT events [Del Pezzo et al. 2004a,b, Madonia et al. 2008]. Most of these earthquakes are located above 4 km below sea level (b.s.l.) inside a volume centered along the crater axis. Depth distribution has a maximum at 2-3 km, in correspondence of the transition between the volcanic edifice and the carbonatic basement [Scarpa et al. 2002, Del Pezzo et al. 2004a]. The most energetic earthquake occurred on October 9, 1999,

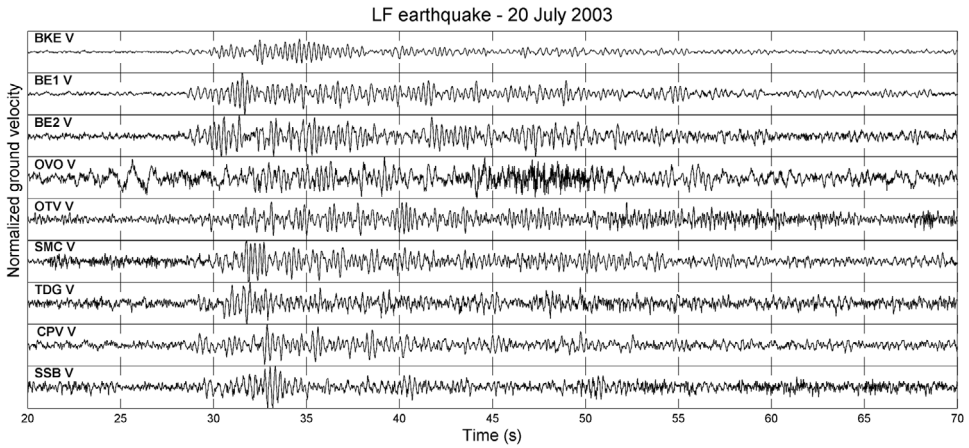

Figure 2. LP event seismograms recorded on the vertical components of Mt. Vesuvius Permanent Seismic stations. On the vertical axis the normalized ground velocity is reported.

about 4 km b.s.l. in correspondence of the crater area, with a duration magnitude M_D 3.6 [Zollo et al. 2002, Del Pezzo et al. 2004a]. The usual source dynamics estimated for vesuvian VT is of Double-Couple (DC) typology, with Strike-slip and normal/reverse Dip-slip focal mechanisms, and nodal planes mainly oriented along the NW–SE and NE–SW directions [Bianco et al. 1998, Ventura and Vilardo 1999]. The main orientations retrieved for the P and T axes are NNE–SSW and ESE–WNW directions, respectively, and ESE–WNW and NNE/N–SSW/S directions, respectively [Bianco et al. 1998, Ventura and Vilardo 1999, Zollo et al. 2002]. Del Pezzo et al. [2004a] showed that the deepest events have an average stress drop in the range 1-10 MPa, with the shallowest events characterized by stress drop of up to 1 MPa. These authors suggested that the shallowest low-stress drop events are triggered by increasing pore fluid pressure generated by changes in the level of the hydrothermal aquifer, whose top is located at about 1 km b.s.l., beneath the crater [Caliro et al. 2011]. Conversely, high-stress drop seismicity is mainly caused by the regional tectonic stress release occurring in the pre-fractured carbonate basement.

3. Instruments and data

On July 2003 the seismic network of Mt. Vesuvius comprised 12 1Hz-geophones, Mark L4C or Geotech S13, of which 5 were three- and 7 single-component. The acquired signals were sampled at 100 Hz.

On June 2003 a small-aperture seismic array was installed on the south-eastern flank of Mt. Vesuvius in proximity of the three-component station BKE (Figure 1), about 1 km from the crater and 800 m a.s.l. Two temporary stations (BE1 and BE2) were installed close to BKE to form a triangular geometry with a maximum aperture of 200 m. In November 2003 an additional vertical seismometer (BE3) was installed. More accurate information is available in Bianco et al. [2005]. Currently the array is no more operative.

In Figure 1 we show the map of the stations that recorded the signals analyzed in this study. 2 of these stations are three-component, BKE and OVO, and 8, including BE1 and BE2, are vertical.

A basic study of the LP event was carried out by

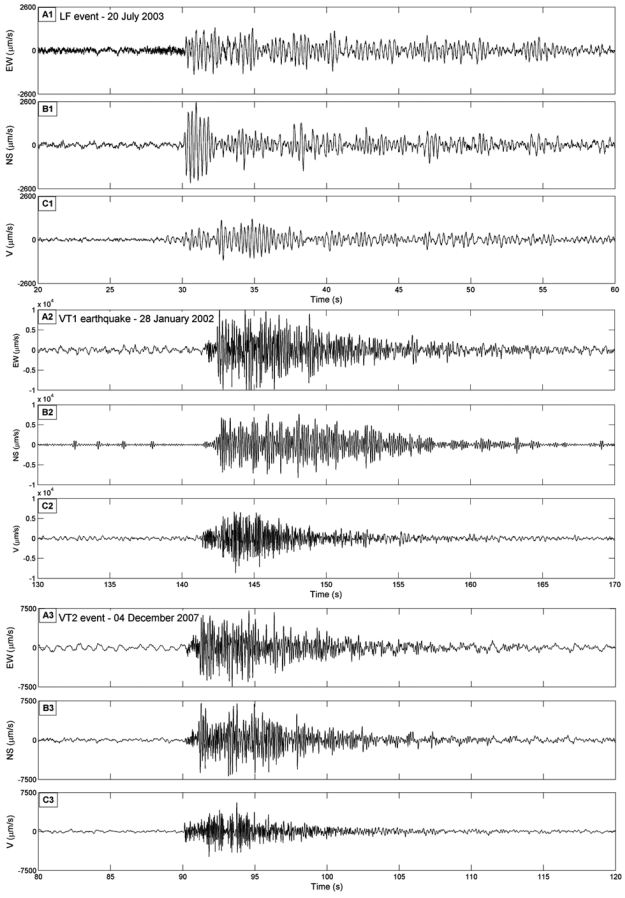

Figure 3. Analyzed event seismograms. 1) The LP event seismograms: A) EW, B) NS and C) V component of ground velocity recorded at BKE station. 2) The VT1 seismograms: A) EW, B) NS and C) V component of ground velocity recorded at BKE station. 3) The VT2 seismograms: A) EW, B) NS and C) V component of ground velocity recorded at BKE station.

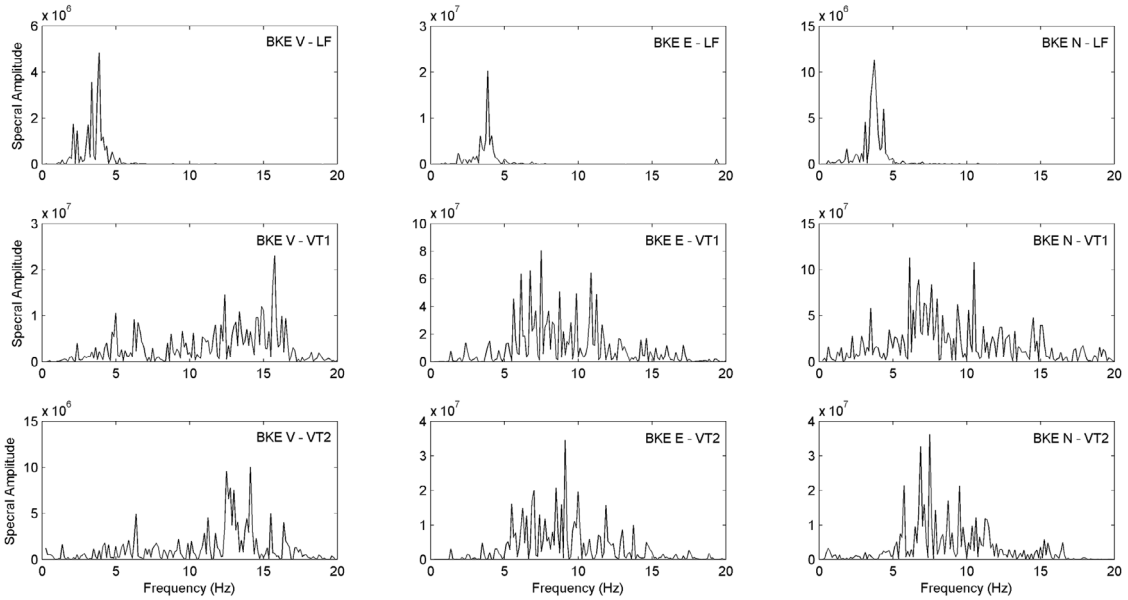

Figure 4. Spectral amplitudes *vs* frequency for the three analyzed events at BKE station. In the upper-right corner of each panel the event and the ground motion component are specified.

Bianco et al. [2005]. Since the location of the LP event is made difficult by the emergent onset of the signal (Figures 2, 3.1), they obtained an acceptable hypocenter position by combining a cross-correlation technique and a 3D-probabilistic procedure (NonLinLoc algorithm [Lomax et al. 2000]; 3D velocity model [Scarpa et al. 2002]). According to this location (Figure 1, red circle) the LP event occurred along the crater axis at a depth of (4.1 ± 0.4) km b.s.l.

With the aim of investigating the nature of the LP event we compared it with test-VT earthquakes. We required that test-VTs must have high quality signals (good signal-to-noise ratio, locatable, signals recoded by all the three-components of BKE station, no amplitude clipping, peculiar and clear spectra) and occurred inside a small volume around the LP hypocenter. We found two suitable candidates:
– January 28, 2002, 09:55 UTC, M_D 1.3, depth (3.8 ± 0.2) km b.s.l., hereinafter VT1 (Figure 3.2);
– December 4, 2007, 02:44 UTC, M_D 0.9, depth (3.5 ± 0.3) km b.s.l., hereinafter VT2 (Figure 3.3).

The reported depths are calculated by using NonLinLoc algorithm (Figure 1, green and blue circle for VT1 and VT2, respectively). The two VTs are characterized by Ts-Tp of about 1 s.

The M_D value for the two VTs was estimated using a relation between the magnitude and the signal duration, expressly calibrated for vesuvian VT earthquakes [Bianco et al. 2005] recorded at the vertical component of OVO station (Figure 1).

Bianco et al. [2005] estimated the Equivalent Duration Magnitude (EDM) for the LP by using a method based on the measurement of the signal amplitude from the displacement spectrum, finding a value of 0.6.

4. Data analysis

We use the three-component BKE station (Figure 1) as reference station for our analyses since it is the closest to the crater and has the best signal/noise ratio.

4.1. Spectral content and coda decay

We compared LP, VT1 and VT2 on the basis of their spectral content. We calculated the amplitude spectra (Figure 4) and spectrograms (Figure 5) (FFT) on 25 s of signal recorded by the three-components of the ground motion at BKE station for the 3 events. The LP event shows a quasi-monochromatic spectral content in 3-4 Hz frequency band (Figure 4; Figure 5, panels LP.1, LP.2 and LP.3). Moreover the LP main frequency content is persistent in time. On the other hand, for the two VTs the energy mostly concentrates in the band 5-10 Hz for all the components (Figure 4 and Figure 5, VT1 and VT2 panels) showing further peaks in 10-15 Hz on the vertical components.

To ensure that local effects do not introduce biases on the results, we calculated the amplitude spectra also for LP, VT1 and VT2 recorded at the three-component OVO station (Figure 6). The spectra of the LP are broader than in the case of BKE (Figure 4), but they remain below 6-7 Hz, with the main peaks around 3-4 Hz, the same frequencies observed at BKE. On the other hand a shift of the most energetic bands toward lower frequencies for the VTs are clearly observed (Figure 4). This shift can be likely attributed to attenuation effects [Bianco et al. 1999].

With the aim to investigate the coda decay, we calculated the envelope of each earthquake at BKE station by estimating the Hilbert Transform in three frequency bands, chosen on the basis of the signal

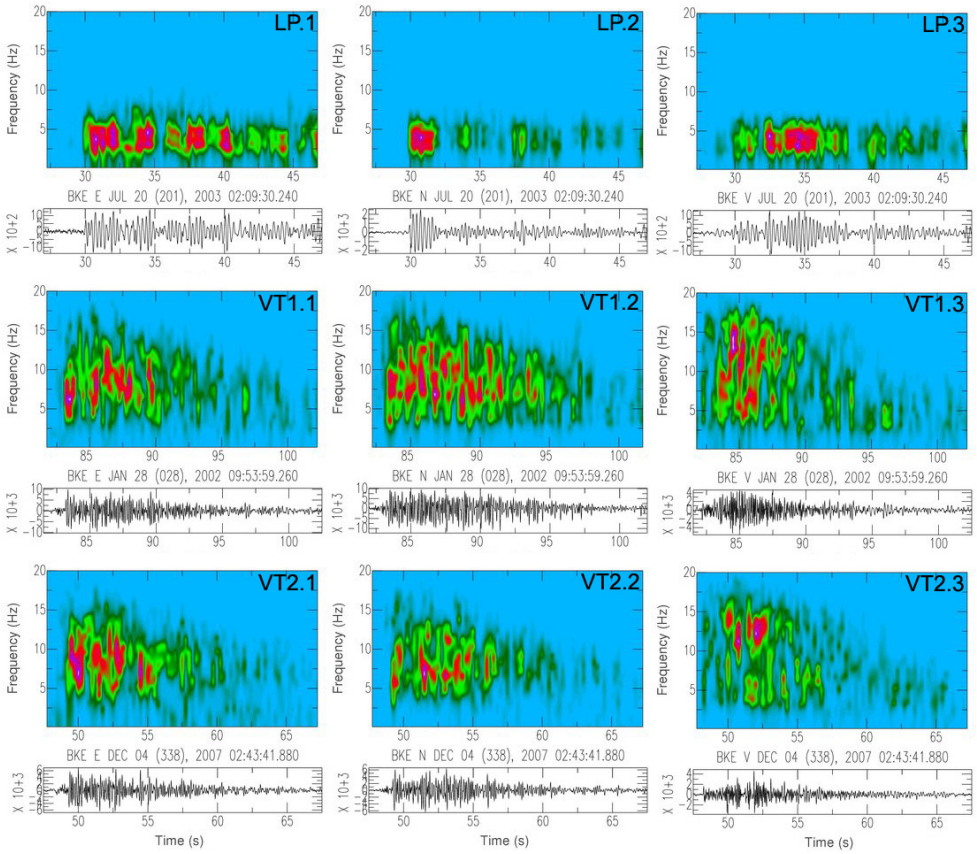

Figure 5. In each panel the spectrogram (upper graph) and the trace (bottom graph) refer to the specified component of BKE station. The spectrograms are represented with a normalized color scale, from blue (lower values) to purple (higher values). The panels numbered with 1, 2 and 3 refer to the EW, NS and V component respectively.

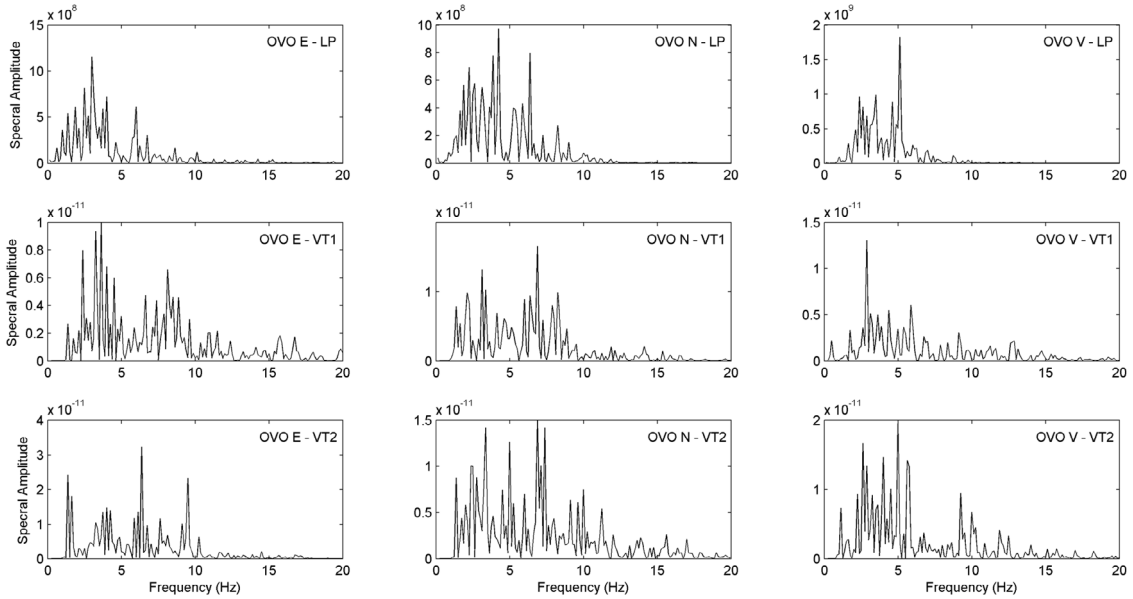

Figure 6. Spectral amplitudes *vs* frequency for the three analyzed events at OVO station. In the upper-right corner of each panel the event and the ground motion component are specified.

spectral content: 1-15 Hz, 1-5 Hz and 5-15 Hz. We calculated the natural logarithm of the envelopes and applied a smoothing algorithm (Figure 7, EW component). Then we synchronized the envelopes respect to the P-wave onset (Figure 7, light gray vertical lines), T_P, and calculated the theoretical starting time of the coda-waves, T_C, as two times the S-wave travel time. Since the three earthquakes share the same source volume, the T_C-T_P values are very close and we assigned the mean, T_C-T_P = 3.66 s, as unique value for the three

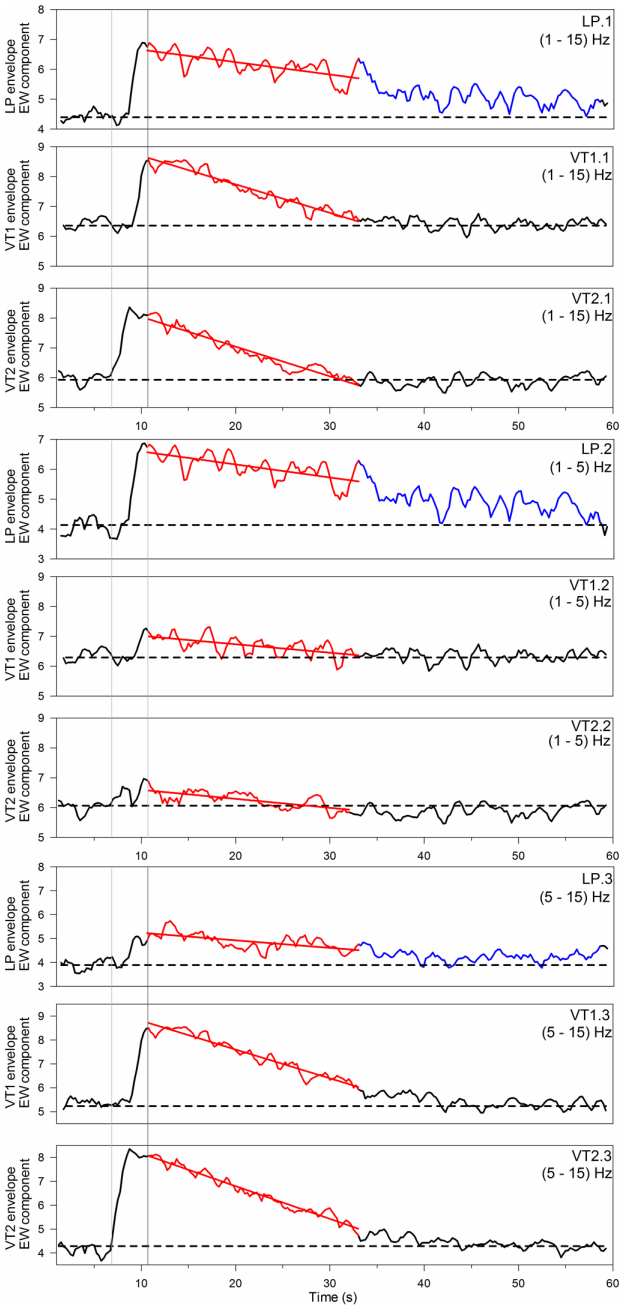

Figure 7. Comparison of the natural logarithms of the envelopes of the EW component for the three events. Three frequency bands are shown, as indicated in the upper-right corner of each panels. The black dashed lines indicate the logarithm of the mean noise envelope in each frequency band, estimated over a time interval of 10 minutes. The vertical light gray lines mark the P-onset, while the dark gray lines mark the coda theoretical starting time. The red lines evidenced the coda envelopes used for the comparison, with their linear fits, while blue lines highlight the actual LP coda.

Event	(1-15) Hz	(1-5) Hz	(5-15) Hz
LP	-0.041 ± 0.005	-0.043 ± 0.005	-0.031 ± 0.004
VT1	-0.10 ± 0.01	-0.028 ± 0.003	-0.12 ± 0.01
VT2	-0.10 ± 0.01	-0.032 ± 0.003	-0.14 ± 0.01

Table 1. Slopes and associated errors obtained for the EW component of BKE station.

earthquakes (Figure 7, dark gray vertical lines). We compared the coda decay for the three earthquakes by calculating the slopes of the linear fits (Figure 7, the least mean square, red lines) of the coda logarithm envelopes. The duration considered for the coda analysis was fixed at 22 s (Figure 7, red lines) by considering that VT1 has a total duration of 27 s and VT2 of 25 s, and the LP is longer (Figure 3). From the estimated slopes and the associated errors (reported in Table 1 for the EW component) the following observations can be done:

– The two VTs have the same slope in all the frequency bands;

– The LP slope is significantly different from the two VTs'.

These observations are indicative of a different phenomenon in the generation of the LP signal respect to a typical VT.

Moreover the envelope of LP results above the mean noise level (Figure 7, dashed black lines) well over the duration of the two VTs (Figure 7, blue lines) in each frequency band. This signature is frequently observed in Long Period seismicity of other volcanoes [Chouet 1988, Jolly et al. 2012].

4.2. Source characteristics

We performed a Seismic Moment Tensor (SMT) inversion for the LP event using the technique developed by Herrmann and Ammon [2002]. We assumed a point source and performed the inversion of the waveforms in the time domain for the first 2 s of signals after the P-wave onset. We used the signals from the 9 stations, 2 of which are three-components, that operated in that period. The windowed signals were filtered in the 1-5 Hz frequency band. Green functions for double-couple and explosive sources in the depth range 0-6 km b.s.l. in 1D-layered velocity model (adapted from the 3D model of Scarpa et al. [2002]) were generated. Synthetic signals were cut and filtered as the observed signals. We performed a full unconstrained inversion for SMT and depth, in the depth range 0-6 km. The goodness of each solution is evaluated by the comparison between the observed signals and the synthetics generated by a test source, quantified by the variance reduction parameter:

$$\sigma^2 = 1 - \frac{\sum (s_i - d_i)^2}{\sum (s_i)^2} \qquad (1)$$

where s_i is i-th synthetic sample and d_i i-th real sample. The more σ^2 is close to 1, the more the synthetics reproduce the real signals. In our case the best solution has a σ^2 of 0.6 and corresponds to a depth of 3.8 km, compatible with the hypocenter depth retrieved with the 3D location. We are aware that the retrieved best source

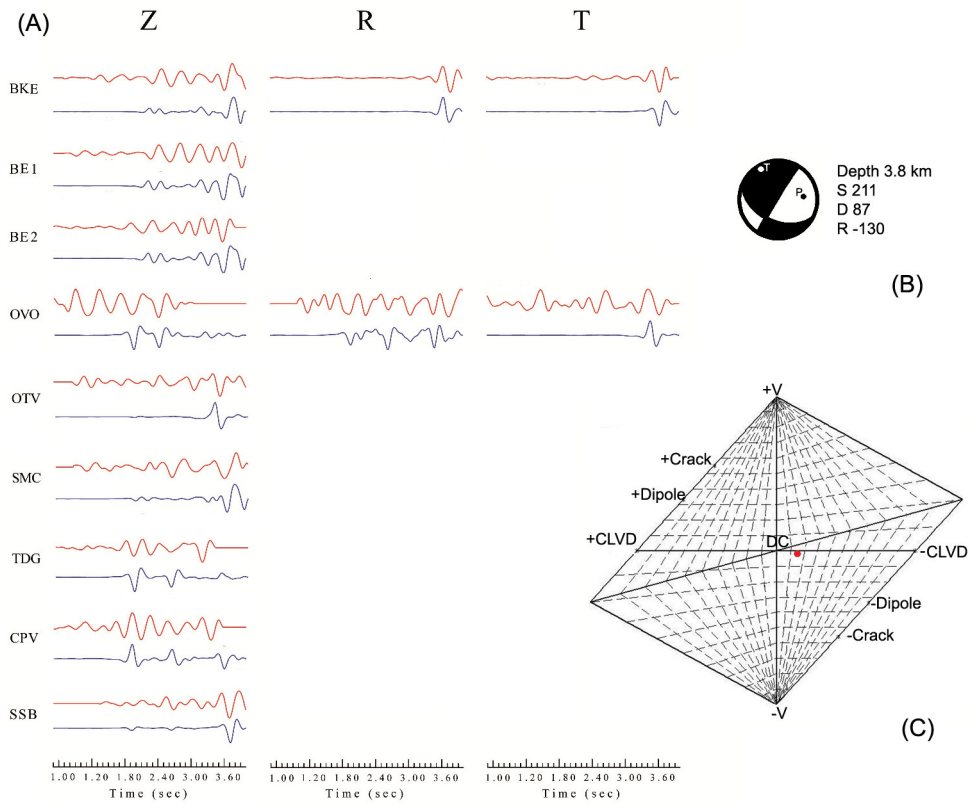

Figure 8. Seismic Moment Tensor inversion results. (A) Comparison between the real seismic signals (red lines) of the LP event and the synthetics (blue lines) generated for the best source retrieved by the inversion. Z is the vertical, R the radial and T the transversal component of the ground velocity. (B) The retrieved double couple mechanism is reported with the associated geometric parameters (S = strike, D = dip and R = rake). P (compressional) and T (tensional) axes are indicated. (C) Source-Type Plot of k (vertical coordinate) and T (horizontal coordinate) parameters. The loci for pure DC, CLVD, dipole, crack and isotropic (V) source are marked. The red circle corresponds to the k and T values calculated for the LP event.

modeling with $\sigma^2 = 0.6$ is able to reproduce the observed signals quite well with the following limitations:
– We used a simplified velocity model not including the topography;
– In the inversion procedure we considered Green function generated by double couple and explosion point forces;
– A high level of noise affects the entire seismic network, also in the frequency band of interest.

In Figure 8C we show the SMT components resulted from the inversion on a Source-Type Plot [Hudson et al. 1989]. In this representation, the ratio of the principal moments (components) defines the position of the point that is associated with a given source mechanism. The horizontal (T) and vertical (k) coordinates are defined as

$$T = \frac{m_1}{|m_3|}, \quad k = \frac{m^v}{|m^v| + |m_3|} \qquad (2)$$

where m_1 and m_3 are the smallest and the largest deviatoric principal moments, respectively, and m^v is the isotropic one. According to this definition, the horizontal coordinate is linked to a Compensated Linear Vector Dipole (CLVD) source type, while the vertical component is a measure of the volume change. The advantage of this representation is that the parameters T and k are independent from non-unique decompositions of the SMT. The figure shows that our solution is very close to a pure DC, meaning that the source dynamics is dominated by a fracture mechanism.

We checked the stability of SMT inversion result through a jackknife test [Efron 1982, Dreger et al. 2000], a resample method in which all the possible subsets of the data are inverted to evaluate if a certain station or a combination of stations control the inversion. If the total number of station is N, all the possible subsets are composed by N-j stations, with $j = 1, \ldots, N$-3, without duplications. Fixed the source depth value, we assumed that the SMT solution for all the stations is approximately the true solution. For each combinations of the N-j stations we calculated DC, ISO and CLVD mean percentages and their standard deviation. We found that the means tend to asymptotic values which indicates a poor influence of local biases on the solution and a scarce dependence on the azimuth.

The comparison between the observed signals and the synthetics generated for the retrieved source is reported in Figure 8A, together with the stereographic projection associated with the double couple (DC) source mechanism and the relative fault geometrical parame-

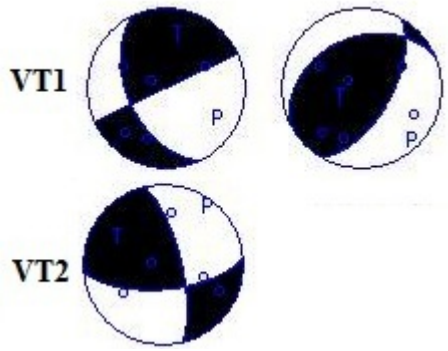

Figure 9. Focal mechanisms calculated for VT1 (up) and VT2 (bottom). P and T axes are indicated.

ters (B). This plot shows a general good agreement between observed and synthetic signals, especially for the S-phases on the radial and transversal components of BKE station. The fit gets worse as the distance from the crater increases, probably due to the contamination of path effects. The worst fit corresponds to OVO station, likely caused by the low signal-to-noise ratio. The calculated DC mechanism is compatible with the local stress field (see Section 2):

– nodal plane strike about 210° or 120° (NE-SW or SE-NW);

– compressional (P) axis trend ~90° (compatible with ESE-WNW);

– tensional (T) axis trend ~330° (compatible with N-S).

We also tried to perform the inversion of the two VTs' waveforms filtered in 1-5 Hz frequency band, but the corresponding σ^2 values resulted less than 0.1.

On the other hand, since the two VTs have clear P-wave onsets (Figures 3.2C, 3.3C), we were able to calculate their focal mechanisms from P-wave polarities using the standard grid-search code FPFIT [Reasenberg and Oppenheimer 1985]. We found two solutions, a right-lateral strike-slip and a thrust, for VT1 (Figure 9, upper plot). Although the right-lateral strike-slip is more usual for the vesuvian VTs, both mechanisms are compatible with the local stress field and hence we have no elements to discard one or the other. For VT2 we found a left-lateral strike-slip faulting (Figure 9, bottom plot), another common mechanism for Mt. Vesuvius.

5. Discussion and conclusions

LP earthquakes, together with volcanic tremor, constitute powerful indicators for hazard assessment, since their associated signals are usually observed before and during the eruptions. The underling dynamics is a very difficult task because it concerns the coupling between hydrothermal/magmatic fluids and rock, even though their link to fluid circulation and pressure variations caused by physical-chemical processes is widely recognized. In the present paper we have further investigated the nature of the Vesuvian LP event comparing its features with those of two typical VTs. The ideal candidates for this comparison are obviously earthquakes that occurred in a volume close to the LP source and with comparable magnitude. Unlike the standard VTs, the LP shows a monochromatic long-duration coda (Figures 6, 7), that is a peculiarity of LP seismicity observed in volcanic environment and is generally attributed to fluid filled crack resonance (eigen-oscillations) [Chouet 1988, Lahr et al. 1994, Neuberg et al. 2000, Jolly et al. 2012].

The SMT inversion results indicate that the first 2 seconds of the signals are generated by a dominating fracturing process that, in turn, could indicate that the July 20, 2003, earthquake is an Hybrid earthquake [Chouet 1988, Lahr et al. 1994, Neuberg et al. 2000, Harrington and Brodsky 2007, Jolly et al. 2012]. Even though the SMT retrieved fault mechanism is compatible with the local stress field (Figure 8), this interpretation leads to some inconsistencies. Hybrid events generally show an impulsive high frequency onset, typical of rock fracturing, that is absent in this earthquake. This lack cannot be attributed to an attenuation effect since we find the presence of high frequency peaks in the P-wave of very low energy earthquakes ($M_D = 0.4$) generated at depths in the range 3.5-4.1 km b.s.l. at Mt. Vesuvius in 1999. As an example in Figure 10 we show the seismogram and the amplitude spectrum of the $M_D = 0.4$ VT recorded on December 19, 1999, at BKE station, that was only vertical-component at that time. This earthquake was located at 4.1 ± 0.2 km of depth and its spectrum shows clear high frequency peaks, with the highest at 16 Hz. More-

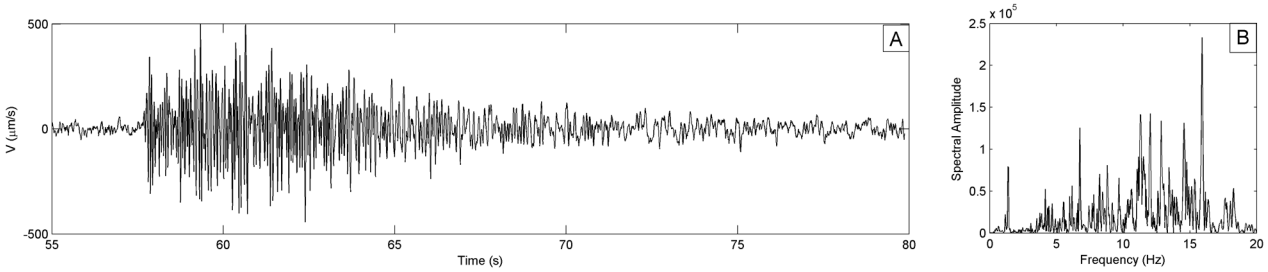

Figure 10. Seismogram (A) and the amplitude spectrum (B) of the $M_D = 0.4$ VT recorded on December 19, 1999, at BKE station (vertical component only at the time of the recording).

over we exclude that a low-velocity rupture [Harrington and Brodsky 2007] could have generated the July 20, 2003, earthquake since for such mechanism a coda decay with the same rate of VTs is expected because coda duration would be the result of path effects rather than of the source. It is likely that the uncertainties which affect the SMT analysis are too large to obtain a reliable result. Possibly the medium of propagation is too much complex for the approximations made to generate the Green's functions. We remark that the Green's functions were generated for a 1D-layered velocity model and without taking into account the topographic effect.

It seems more plausible that the unique Vesuvian LP earthquake involves the classical model of eigen-oscillations of a fluid-filled crack on the basis of the waveform and the spectral content. The presence of hydrothermal fluids, namely brines, at the depth of the event hypocenter is settled in the conceptual geochemical model of the volcanic system of Vesuvius depicted by Caliro et al. [2011]. Moreover perturbations in the deep fluid system at Mt. Vesuvius in coincidence with the LP occurrence are evidenced by the groundwater analysis of Federico et al. [2013]. The Vesuvian hydrological system consists of two main circuits, the northern, more indicative of the shallower fluids, and the southern, more influenced by the deep water, with a strong contribution from the brine [Federico et al. 2002]. The mid-2003 was characterized by many contemporary anomalies in the water chemistry (water temperature, HCO_3, NO_3, SO_4/HCO_3) in some wells and one spring of the southern sector. These observations are in agreement with the composition changes in the magmatic volatiles of the crater rim fumarole (He and CO_2), observed by Caliro et al. [2011]. Federico et al. [2013] suggest that these anomalies can be ascribed to a deep pressure drop occurred during the phase of exhaustion of degassing of the deep fluids. The generation of the LP seismic event could be linked to this drop of fluid pressure.

The uniqueness of the July 20, 2003, earthquake is a limitation for our model since a statistics concerning any type of LP seismicity detected in the investigated area does not exist. Nevertheless, this work intends to be a first step toward the construction of such a statistics, and to give a term of comparison for the eventual future occurrence of LP seismicity.

References

Acocella, V., and R. Funiciello (2006). Transverse systems along the extensional Tyrrhenian margin of central Italy and their influence on volcanism, Tectonics, 25 (2); doi:10.1029/2005TC001845. ISSN: 0278-7407.

Bianco, F., M. Castellano, G. Milano, G. Ventura and Vilardo (1998). The Somma-Vesuvius stress field induced by regional tectonics: Evidences from seismological and mesostructural data, J. Volcanol. Geoth. Res., 82, 199-218; doi:10.1016/S0377-0273(97)00065-6.

Bianco, F., M. Castellano, E. Del Pezzo and J.M. Ibanez (1999). Attenuation of short-period seismic waves at Mt. Vesuvius, Italy, Geophys. J. Int., 138, 67-76; doi: 10.1046/j.1365-246x.1999.00868.x.

Bianco, F., P. Cusano, S. Petrosino, M. Castellano, C. Buonocunto, M. Capello and E. Del Pezzo (2005). Small-aperture Array for Seismic Monitoring of Mt. Vesuvius, Seismol. Res. Lett., 76, 344-355; doi: 10.1785/gssrl.76.3.344.

Caliro, S., G. Chiodini, R. Avino, C. Minopoli and B. Bocchino (2011). Long time-series of chemical and isotopic compositions of Vesuvius fumaroles: evidence for deep and shallow processes, Annals of Geophysics, 54 (2); doi: 10.4401/ag-5034.

Chiodini, G., L. Marini and M. Russo (2001). Geochemical evidence for the existence of high-temperature hydrothermal brines at Vesuvio volcano, Italy, Geochim. Cosmochim. Acta, 65, 2129-2147.

Chouet, B.A. (1988). Resonance of a Fluid-Driven Crack: Radiation Properties and Implications for the Source of Long-Period Events and Harmonic Tremor, J. Geophys. Res., 93 (B5), 4375-4400; doi:10.1029/JB093iB05p04375.

Chouet, B.A. (1996). Long-period volcano seismicity: its sources and use in eruption forecasting, Nature, 380 (6572), 309-316; doi:10.1038/380309a0.

Cioni, R., P. Marianelli and R. Santacroce (1998). Thermal and compositional evolution of the shallow magma chambers of Vesuvius: Evidence from pyroxene phenocrysts and melt inclusions, J. Geophys. Res., 103, 18277-18294; doi:10.1029/98JB01124.

Del Pezzo, E., F. Bianco and G. Saccorotti (2004a). Seismic source dynamics at Vesuvius volcano, Italy, J. Volcanol. Geoth. Res., 133, 23-39; doi:10.1016/S0377-0273(03)00389-5.

Del Pezzo, E., F. Bianco, S. Petrosino and G. Saccorotti (2004b). Changes in the Coda Decay Rate and Shear-Wave Splitting Parameters Associated with Seismic Swarms at Mt. Vesuvius, Italy, Bull. Seismol. Soc. Am., 94 (2), 439-452; doi:10.1785/0120030141.

De Vivo, B., and G. Rolandi (2001). Mt. Somma-Vesuvius and volcanism of the Campanian Plain, Mineral Petrol, 73, 233.

Di Renzo, V., M.A. Di Vito, I. Arienzo, L. Civetta, M. D'Antonio, F. Giordano, G. Orsi and S. Tonarini (2007). Magmatic history of Somma-Vesuvius on the basis of new geochemical and isotopic data from

a deep borehole (Camaldoli della Torre), J. Petrol., 48 (4), 753-784; doi:10.1093/petrology/egl081.

Dreger, D.S., H. Tkaleiæ and M. Johnston (2000). Dilatational processes accompanying earthquakes in the Long Valley caldera, Science, 288, 122-125; doi:10.1126/science.288.5463.122.

Efron, B. (1982). The Jackknife, the Bootstrap and Other Resampling Plans (CBMS-NSF Regional Conference Series in Applied Mathematics, Monograph 38), Philadelphia, SIAM.

Federico, C., A. Aiuppa, P. Allard, S. Bellomo, P. Jean-Baptiste, F. Parello and M. Valenza (2002), Magma-derived gas influx and water-rock interactions in the volcanic aquifer of Mt. Vesuvius, Italy, Geochim. Cosmochim. Acta, 66, 963-981; doi:10.1016/S0016-7037(01)00813-4.

Federico, C., P. Madonia, P. Cusano and S. Petrosino (2013). Groundwater geochemistry of the Mt. Vesuvius area: implications for volcano surveillance and relationship with hydrological and seismic signals, Annals of Geophysics, 56 (4), S0447; doi:10.4401/ag-6453.

Harrington, R.M., and E.E. Brodsky (2007). Volcanic hybrid earthquakes that are brittle-failure events, Geophys. Res. Lett., 34, L06308; doi:10.1029/2006GL028714.

Herrmann, R.B., and C.J. Ammon (2002). Computer programs in seismology – Source inversion: Users manual, report, St. Louis, Mo., St. Louis Univ.

Hudson, J.A., R.G. Pearce and R.M. Rogers (1989). Source type plot for inversion of the moment tensor, J. Geophys. Res., 94, 765-774; doi:10.1029/JB094iB01p00765.

Jolly, A.D., J. Neuberg, P. Jousset and S. Sherburn (2012). A new source process for evolving repetitious earthquakes at Ngauruhoe volcano, New Zealand, J. Volcanol. Geoth. Res., 215/216, 26-39; doi:10.1016/j.jvolgeores.2011.11.010.

Lahr, J.C., B.A. Chouet, C. D. Stephens, J.A. Power and R.A. Page (1994). Earthquake classification, location, and error analysis in a volcanic environment: implications for the magmatic system of the 1989-1990 eruptions at Redoubt Volcano, Alaska, J. Volcanol. Geoth. Res., 62 (1/4), 137-151; doi: 10.1016/0377-0273(94)90031-0.

Lomax, A., J. Virieux, P. Volant and C. Berge (2000). Probabilistic earthquake location in 3D and layered models: Introduction of a Metropolis-Gibbs method and comparison with linear locations, In: C.H. Thurber and N. Rabinowitz (eds.), Advances in Seismic Event Location, Amsterdam, Kluwer, 101-134.

Madonia, P., C. Federico, P. Cusano, S. Petrosino, A. Aiuppa and S. Gurrieri (2008). Crustal dynamics of Mount Vesuvius from 1998 to 2005: Effects on seismicity and fluid circulation, J. Geophy. Res., 113, B05206; doi:10.1029/2007JB005210.

Neuberg, J., R. Luckett, B. Baptie and K. Olsen (2000). Models of tremor and low-frequency earthquakes swarms on Montserrat, J. Volcanol. Geoth. Res., 101 (1/2), 83-104; doi.org/10.1016/S0377-0273(00)00169-4.

Reasenberg, P.A., and D. Oppenheimer (1985). FPFIT, FPPLOT and FPPAGE: Fortran computer programs for calculating and displaying earthquake fault-plane solutions, Open-File Report No. 85-739, U.S. Geological Survey.

Scarpa, R., F. Tronca, F. Bianco and E. Del Pezzo (2002). High resolution velocity structure beneath Mount Vesuvius from seismic array data, Geophys. Res. Lett., 29 (21), 2040; doi:10.1029/2002GL015576.

Ventura, G., and G. Vilardo (1999). Slip tendency analysis of the Vesuvius faults: Implications for the seismotectonic and volcanic hazard assessment, Geophys. Res. Lett., 26 (21), 3229-3232; doi:10.1029/1999GL005393.

Zollo, A., W. Marzocchi, P. Capuano, A. Lomax and G. Iannaccone (2002). Space and time behavior of seismic activity at Mt. Vesuvius volcano, southern Italy, Bull. Seismol. Soc. Am., 92 (2), 625-640; doi: 10.1785/0120000287.

*Corresponding author: Paola Cusano,
Istituto Nazionale di Geofisica e Vulcanologia, Sezione di Napoli, Osservatorio Vesuviano, Naples, Italy;
email: paola.cusano@ov.ingv.it.